Electronic Supplementary Material (ESI) for Environmental Science: Nano.

Biomolecular Corona Formation on CuO Nanoparticles in Plant Xylem Fluid

Jaya R. Borgatta,[‡1] Christian A. Lochbaum,[‡1] Wade Elmer,[2] Jason C. White,[2] Joel A. Pedersen,*[1,3] Robert J. Hamers*[1]

[1] Department of Chemistry, University of Wisconsin−Madison, 1101 University Avenue, Madison, Wisconsin 53706, United States

[2] Department of Plant Pathology and Ecology, The Connecticut Agricultural Experiment Station, 123 Huntington Street, New Haven, Connecticut 06504, United States

[3] Departments of Soil Science and Civil & Environmental Engineering, University of Wisconsin−Madison, 1525 Observatory Dive, Madison, Wisconsin 53706, United States

[‡] Authors contributed equally

* Authors to whom correspondence should be addressed

Contents

Experimental

Figure S1. Collection of xylem fluid from a cut stem of a pumpkin plant.

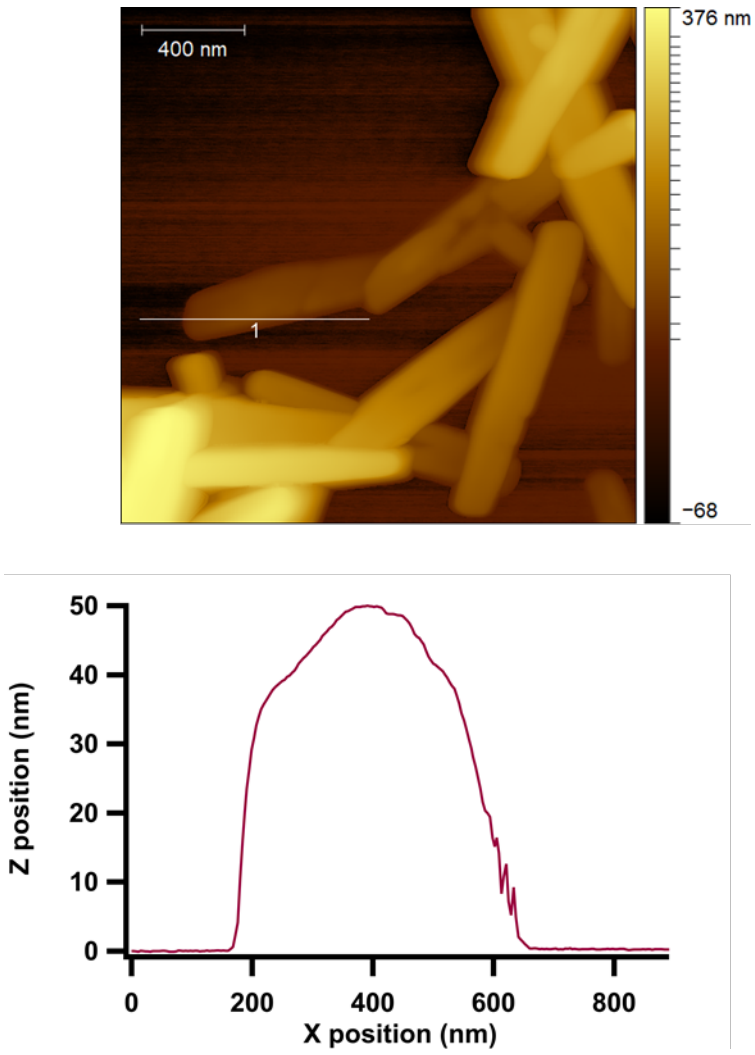

Figure S2. Atomic force microscope image of CuO nanoparticles on a mica substrate. The line labeled 1 corresponds to the line scan plot displayed below. The line scan indicates that the maximum nanoparticle height is approximately 50 nm.

Calibration curve for total carbohydrate assay. Calibration of total carbohydrate assay was performed with 0, 25, 50, 100, 150, and 300 $mg \cdot L^{-1}$ glucose standards. The assay was performed by combining 200 µL of 5% w/v phenol in water solution with 250 µL of standard in a glass vial. A 1 mL volume of 98% sulfuric acid was rapidly added and the solution was vortexed briefly. The solution was left to cool for 1 hour and the absorbance was measured at 460 nm using a BioTek Synergy 2 plate reader. Three replicate measurements were performed for each concentration of glucose. A calibration curve was generated for each 96 well plate separately (Figure S3).

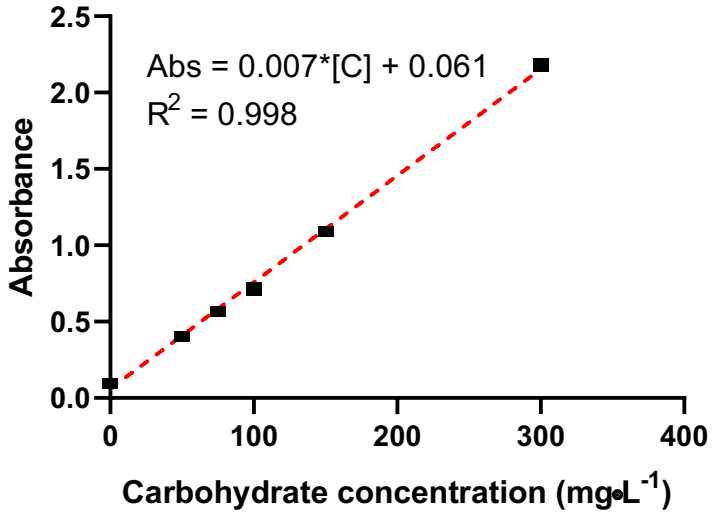

Figure S3. Absorbance measurements for 0, 25, 50, 100, 150, and 300 mg·L^{-1} ppm glucose standards. Dotted red line is a linear fit of glucose concentration vs absorbance. Linear fit for glucose concentration vs absorbance was good with an R^2 of 0.998. Error bars represent one standard deviation of three replicate measurements.

Calibration curve for total protein assay. Calibration of total protein assay was performed with 0, 5, 25, 50, 125, and 250 mg·L^{-1} bovine serum albumin (BSA) standards. Quantification of protein in solution was performed using a Pierce™ BCA Assay Kit was purchased from Thermo Scientific (product number 23225). To use the kit 25 µL of sample was added to 200 µL working reagent in a 96-well plate, incubated for 30 min at 60 °C, and absorbance was measured at 562 nm using a BioTek Synergy 2 plate reader. Three replicate measurements were performed for each concentration of glucose. A calibration curve was generated for each 96-well plate separately (Figure S4).

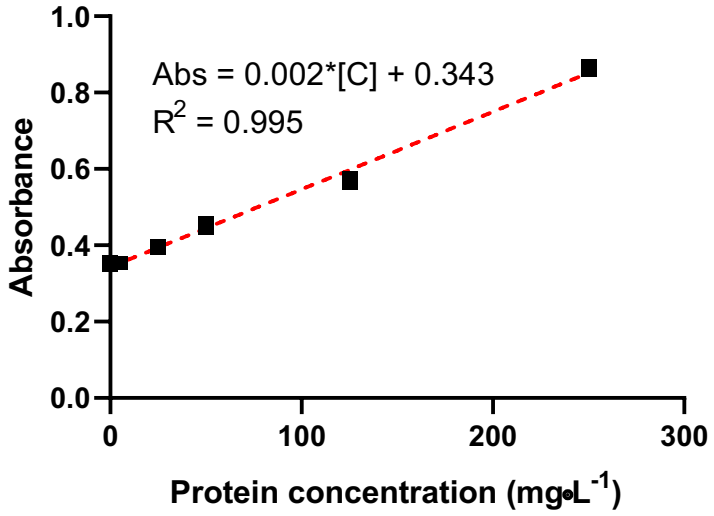

Figure S4. Absorbance measurements for 0, 5, 25, 50, 125, and 250 mg·L^{-1} BSA standards after BCA treatment. Red dotted line represents a linear fit of protein concentrations vs absorbance. Linear fit for protein concentration vs absorbance was good with an R^2 of 0.995. Error bars represent one standard deviation of three replicate measurements. There was no significant difference between 0 and 5 mg·L^{-1} standards ($p > 0.05$).

In situ ATR-FTIR spectroscopy of model molecules interacting with CuO nanoparticles. The nanoparticle films were prepared as described in the methods section. The internal reflection element with the nanoparticle film was then installed in the flow cell and allowed to equilibrate in ultrapure water (18 MΩ) for ~1.5 hours. The solution of interest was then flowed over the nanoparticle film and spectra were collected. The ubiquitin, dextran, and malic acid were purchased from Millipore Sigma and used without further purification. The 1,2-dioleoyl-*sn*-glycero-3-phosphocholine (DOPC) was obtained from Avanti polar lipids (item number 850375).

Results and Discussion

Xylem fluid viscosity. Estimated viscosity of xylem fluid is between 8.90×10^{-4} Pa·s (the viscosity of water at 25 °C) and 1.2×10^{-3} Pa·s. [1, 2] The viscosity of xylem fluid may therefore be higher than that of water, leading to a smaller diffusion coefficient in xylem fluid than in water for the same sized particle according to the Stokes-Einstein equation:

$$D = \frac{k_B T}{6\pi\eta a}$$

where k_B is the Boltzmann constant, T is absolute temperature, η is dynamic viscosity, and a is particle radius. Using the maximum estimated value of xylem fluid viscosity (1.2×10^{-3} Pa·s), the Stokes-Einstein equation indicates that the diffusion coefficient of CuO NPs in xylem fluid could be lower than that in water by a factor of 0.74. The measured diffusion coefficients of CuO NPs in water and xylem fluid was 1.18 ± 0.03 μm^2·s^{-1} and 0.32 ± 0.04 μm^2·s^{-1} respectively; that is, the diffusion coefficient in xylem fluid was

lower than that in water by a factor of 0.27. This difference is larger than can attributable to the higher viscosity of xylem fluid than water.

CuO NP electrophoretic mobility. The ionic strength of xylem fluid is 32 ± 14 mM (*Ricinus communis*) [3] is significantly larger than ionic strength of water (estimated to be 1 x 10^{-7} M). To estimate the effect of changing ionic strength from water to xylem fluid, we used Henry's equation: [4]

$$\mu_e = \frac{2\varepsilon\zeta F(\kappa a)}{3\eta}$$

where μ_e is the electrophoretic mobility, ε is the solvent dielectric permittivity, ζ is the zeta potential, $F(\kappa a)$ is Henry's function, and κ is the inverse Debye length. Henry's function was calculated for using Ohshima's relation[5] for water (1.00) and xylem fluid (1.39). This was combined with the Debye-Hükel approximation: [4]

$$\sigma = \frac{\epsilon\zeta(1+\kappa a)}{a}$$

By solving for ζ in the Debye-Hükel equation and combining with Henry's equation, we estimated the impact of xylem fluid ionic strength on CuO NP electrophoretic mobility. Using the maximum estimated value of xylem fluid viscosity (1.2×10^{-3} Pa·s) and the median value of xylem fluid ionic strength (32 mM), Henry's equation indicates that the electrophoretic mobility of CuO NPs in xylem fluid could be lower than that in water by a factor of 0.04. The measured electrophoretic mobility of CuO NPs in water and xylem fluid was +2.7 ± 0.6 $cm^2 \cdot mV^{-1} \cdot s^{-1}$ and +0.2 ± 0.3 $cm^2 \cdot mV^{-1} \cdot s^{-1}$ respectively; that is, the electrophoretic mobility in xylem fluid was lower than that in water by a factor of 0.07. This difference is within the range attributable to ionic strength change.

Calculating organic layer thickness. The approximate thickness of an overlayer on a substrate was determined using measurements of the N and Cu peak areas. [6] The detection of an electron from a specific element is influenced by the number density of the material (ρ), the sensitivity factor of the XPS instrument for that element (SF), the inelastic mean free path of an electron traveling through that material (λ), the angle of the detector with respect to the surface normal (θ), and the thickness of the material (z). The overall effects of electron scattering within the bulk CuO substrate (sub) and the overlayer can be described as:

$$\frac{(1-e^{-z/\lambda_{overlayer}cos\theta})}{e^{-z/\lambda_{Sub\ through\ overlayer}cos\theta}} = \frac{A_{overlayer}\,\rho_{sub}\,SF_{sub}\,\lambda_{sub}}{A_{sub}\,\rho_{overlayer}\,SF_{overlayer}\,\lambda_{overlayer}} \quad \text{(S1)}$$

The unknown side is then plotted as a function of thickness creating plots like the one displayed in Figure S5. The number density of CuO was calculated to be 47.84 molecules·nm^{-2}. The number density of adsorbed N from protein was determined using the following expression:

$$Number\ density\ N = \frac{\rho_{protein} \times N_A \times Number\ of\ N\ atoms\ in\ the\ amino\ acid\ backbone}{MolarMass_{amino\ acid}}$$

where the molar mass of amino acids is 110 g·mol^{-1} (the average molecular mass of all the amino acids), $\rho_{protein}$ is the density of protein is 1.35 g·cm^{-3}, N_A is the Avogadro constant, and the number of N atoms in the amino acid back bone is 1. The NIST standard reference database 71 was used to determine the inelastic mean free path (IMFP). [7] Since the identity of the proteins bound to the CuO is not known, BSA was used as a reference protein. [8] To perform the IMFP calculations the density of protein was assumed

to be 1.35 g·cm^{-3} and a density of CuO was 6.31 g·cm^{-3} was used for CuO. To determine the energy-dependent IMFP, we used electron kinetic energies of 553 eV for Cu, 1202 eV for C(1s), and 1087 eV for N(1s). The inelastic mean free path for photoelectrons were estimated to be 1.2 nm for Cu(2P) in CuO, and 3.269 nm for N(1s) electrons in the protein layer. We used the following relationship to calculate the 2.07 nm inelastic mean free path of a Cu electron through the protein layer.

$$\frac{\lambda_1}{\lambda_2} = \left(\frac{KE_1}{KE_2}\right)^{0.67} \quad \text{(S2)}$$

The right side of equation S1 was then solved for using the experimental parameters and the value was then plotted to determine the layer thickness of protein.

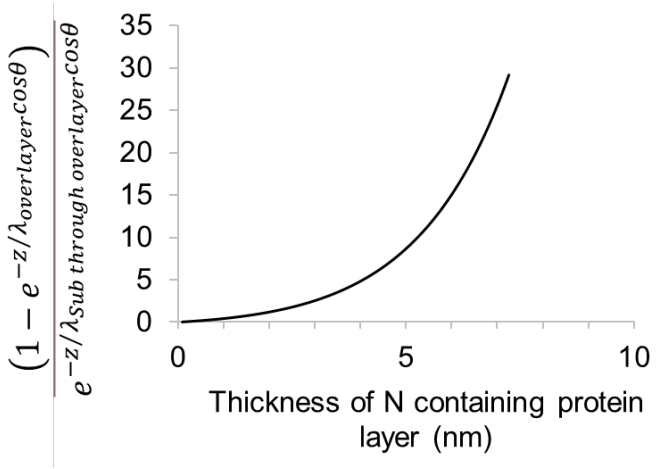

Figure S5. Plot of attenuation as a function of N containing protein layer thickness as calculated using equation S1. Attenuation factor refers to the right-side of equation S1.

*Estimating protein removal from corona thickness***.** Corona thickness, as determined by XPS, was used to estimate protein removal from solution. The estimated protein removal was compared to experimental protein removal to show agreement between the BCA and XPS approaches. Particles were approximated as rectangular prisms of 900 nm × 120 nm × 50 nm for surface area and concentration calculations.

$$Surface\ Area = (900\ nm \times 120\ nm + 900\ nm \times 50\ nm + 120\ nm \times 50\ nm) \times 2$$
$$= 3.18 \times 10^5 \frac{nm^2}{particle}$$

$$Volume = 900\ nm \times 120\ nm \times 50\ nm = 5.4 \times 10^6 \frac{nm^3}{particle}$$

For the 50 and 1000 mg·L^{-1} CuO concentration the corona thickness from XPS was estimated to be 5.1 and 1.9 nm respectively. Here we outline the approximation of protein depletion that would create a uniform corona of 1.9 nm thickness on 1000 mg·L^{-1} CuO NPs. The same calculation was performed for a corona of 5.1 nm thickness on 50 mg·L^{-1} CuO NPs. The density of CuO is 6.31 g·cm^{-3}. The exposed surface area was calculated:

$$1000\,\frac{mg}{L}\,CuO\ NPs \times \left(\frac{1\ cm^3}{6.31\ g}\right) \times \left(\frac{1\ particle}{5.4 * 10^6\ nm^3}\right) \times \left(\frac{3.18 * 10^5\ nm^2}{1\ particle}\right) = 9.2 \times 10^{18}\,\frac{nm^2}{L}$$

The density of protein corona was approximated as 1.35 g·cm^{-3}. The protein required to form the corona was calculated:

$$9.2 \times 10^{18}\,\frac{nm^2}{L} \times 1.9\ nm \times \left(\frac{1.35\ g}{1\ cm^3}\right) = 24\,\frac{mg}{L}$$

The approximated protein depletion for 50 and 1000 mg·L^{-1} CuO NPs was 3.2 mg·L^{-1} and 24 mg·L^{-1} respectively. This estimation aligns very well with our experimentally determined values of 9 ± 18 and 28 ± 5 mg·L^{-1} protein is depleted from xylem fluid.

In situ ATR-FTIR of model molecules interacting with CuO nanoparticles. The spectra of xylem interacting with CuO has major peaks at 1542 cm^{-1} and 1628 cm^{-1}, which are consistent with those in the ubiquitin spectrum that represent the Amide I and Amide II regions. The features between 1456 and 1250 cm^{-1} are also consistent with the carboxylate moieties in the ubiquitin spectrum. The relative peak intensities between 1250 and 1628 cm^{-1} in the xylem spectrum are similar to those in the ubiquitin spectrum. The carboxylate moieties could also be due to the presence of small organic acids. The malic acid sample also shows peaks within the region from 1420 to 1195 cm^{-1} associated with C–O or CO_2^- modes. Small organic acids in the xylem fluid may contribute slightly to the corona that is formed. The peak at 1080 cm^{-1} is in the same region where peaks associated with the C–O-C stretches seen in the dextran carbohydrate and the P–O–C stretches of the 1,2-dioleoyl-*sn*-glycero-3-phosphocholine DOPC lipid occur.

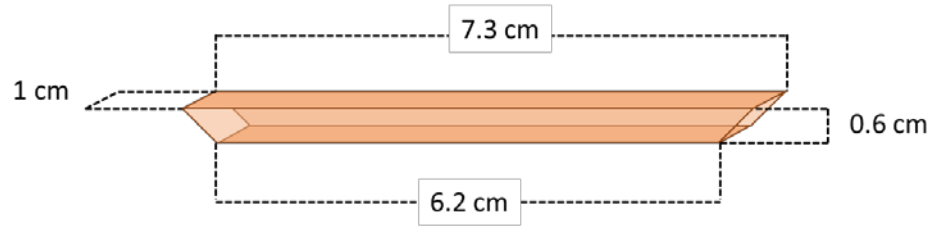

Figure S6. The dimensions of the ZnSe and Ge internal reflectance elements used for *in situ* attenuated total reflectance Fourier-transform infrared spectroscopy experiments.

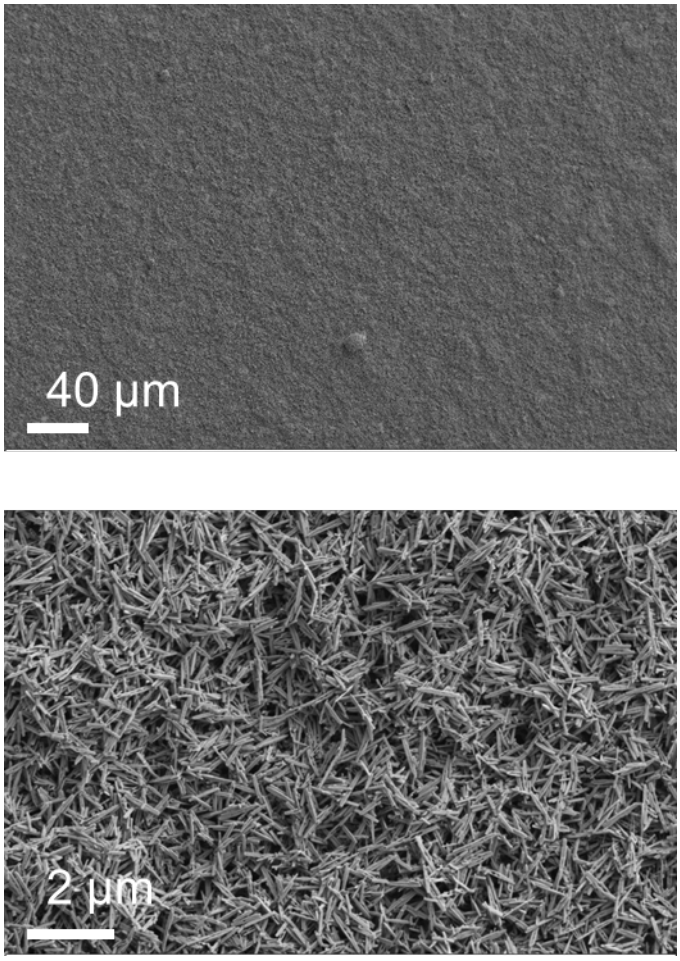

Figure S7. CuO nanoparticles deposited on Ge element showing a uniform, at low magnifications (above) and high magnifications (below).

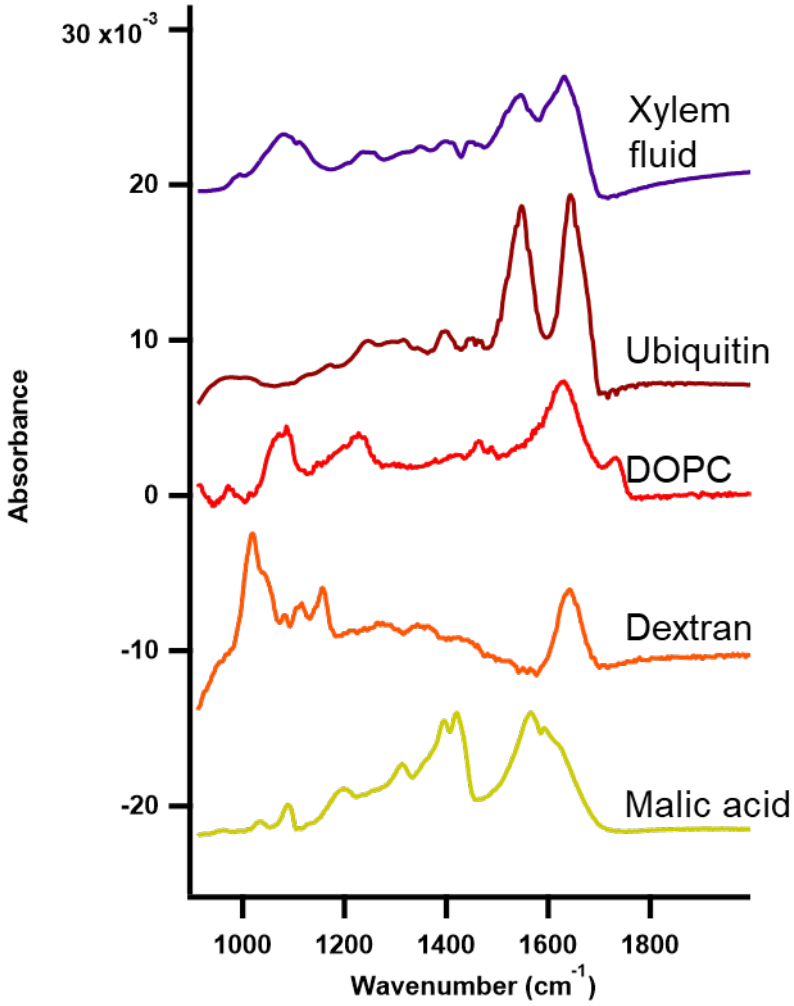

Figure S8. *In situ* ATR-FTIR spectra of model biomolecules interacting with the surface of CuO nanoparticles. The model biomolecules were malic acid to represent small carboxylic acids, dextran to represent carbohydrates, DOPC to represent lipids, ubiquitin to represent proteins, and xylem fluid for reference.

Table S1. Peaks present in the ATR-FTIR spectrum of xylem fluid, showing the presence of carbohydrate, protein, and carboxylate moieties.

Peak position (cm^{-1})	Identity	Associated molecule
1080	C–O , P–O, or P–O–C stretch	Carbohydrate, phospholipid
1150.4	C–O stretch	Carbohydrate
1231.3	Amide III	Protein
1243.9	Amide III	Protein
1348	Carboxylic acid O–H deformation vibration	Carboxylic acid moiety
1394.3	Symmetric CO_2^- stretch	Carboxylic acid moiety
1524.5	Amide II	Protein
1541.8	Amide II	Protein
1636.3	Amide I	Protein
2337.3	CO_2 peak	CO_2
2361.5	CO_2 peak	CO_2
2962.2	C–H stretches for methylene and methyl groups	sp^2 hybridized carbon
3266.9	O–H, amide N–H stretch	Protein, carbohydrate, carboxylic acid, phospholipid

References

1. Thompson, M. V.; Holbrook, N. M., Scaling phloem transport: water potential equilibrium and osmoregulatory flow. *Plant, Cell & Environment* 2003**, 26** , 1561-1577.
2. Su, Y.; Ashworth, V.; Kim, C.; Adeleye, A. S.; Rolshausen, P.; Roper, C.; White, J.; Jassby, D., Delivery, uptake, fate, and transport of engineered nanoparticles in plants: a critical review and data analysis. *Environmental Science: Nano* 2019**, 6,** 2311-2331.
3. Peuke, A. D., Correlations in concentrations, xylem and phloem flows, and partitioning of elements and ions in intact plants. A summary and statistical re-evaluation of modelling experiments in Ricinus communis. *J. Exp. Bot.* 2010**, 61**, 635-55.
4. Lowry, G. V.; Hill, R. J.; Harper, S.; Rawle, A. F.; Hendren, C. O.; Klaessig, F.; Nobbmann, U.; Sayre, P.; Rumble, J., Guidance to improve the scientific value of zeta-potential measurements in nanoEHS. *Environmental Science: Nano* 2016**, 3**, 953-965.
5. Delgado, Á. V.; González-Caballero, F.; Hunter, R.; Koopal, L.; Lyklema, J., Measurement and interpretation of electrokinetic phenomena. *Journal of colloid and interface science* 2007, **309**, 194-224.
6. Cumpson, P. J., The Thickogram: a method for easy film thickness measurement in XPS. *Surface and Interface Analysis* 2000, **29**, 403-406.
7. Powell, C. J.; Jablonski, A., NIST Electron Inelastic-Mean-Free-Path Database 71, Version 1.0. **1999**.
8. Tanuma, S.; Powell, C. J.; Penn, D. R., Proposed formula for electron inelastic mean free paths based on calculations for 31 materials. *Surface Science* 1987**, 192**, L849-L857.